IVYSPRING INTERNATIONAL PUBLISHER

Theranostics

2017; 7(15): 3700-3714. doi: 10.7150/thno.19712

Research Paper

Epiregulin Promotes Lung Metastasis of Salivary Adenoid Cystic Carcinoma

Wen-Wen Yang[1], Lin-Qian Yang[1], Fei Zhao[1], Chu-Wen Chen[1], Li-Hua Xu[1], Jia Fu[2], Sheng-Lin Li[1, 2]✉ and Xi-Yuan Ge[1, 2]✉

1. Department of Oral and Maxillofacial Surgery, Peking University School and Hospital of Stomatology, Beijing, PR China;
2. Central Laboratory, Peking University School and Hospital of Stomatology, Beijing, PR China.

✉ Corresponding authors: Xi-Yuan Ge or Sheng-Lin Li, Central Laboratory, Peking University School and Hospital of Stomatology, 22 South Zhongguancun Avenue, Haidian District, Beijing 100081, PR China. Phone: 86.10.82195537; E-mail: gexiyuan@bjmu.edu.cn (XYG) or kqshlli@bjmu.edu.cn (SLL).

Received: 2017.02.17; Accepted: 2017.06.27; Published: 2017.08.23

Abstract

Salivary adenoid cystic carcinoma (SACC) is a peculiar malignant tumor, characterized by its slow but inexorable growth, with a high incidence of lung metastasis and poor prognosis. Here, we show the upregulated expression of EGFR ligand epiregulin in a subset of SACC cells correlates with lung metastasis and unfavorable outcome in patients with SACC. We found that upregulation of epiregulin in SACC cells induced epithelial-mesenchymal transition by regulating GLI1/E-cadherin. Elevated epiregulin increased the expression of pro-angiogenic factors, such as VEGFA, bFGF, and IL-8. We also show that epiregulin can be delivered via exosomes and was enriched in exosomes derived from epiregulin-overexpressing SACC cells. Furthermore, treating immunodeficient mice with these epiregulin-enriched exosomes greatly enhanced SACC metastasis to lung. These epiregulin-enriched exosomes significantly enhanced angiogenesis in the neighboring tumor microenvironment and increased vascular permeability in the pre-metastatic lung microenvironment *in vivo*. Therefore, epiregulin, as well as epiregulin-containing exosomes, may be a novel target for controlling SACC lung metastasis.

Key words: adenoid cystic cacinoma; epiregulin; lung metastasis; exosomes; pre-metastatic niche

Introduction

Salivary adenoid cystic carcinoma (SACC) arises from the secretory epithelial cells of the salivary glands. It account for ~25% of malignant tumors in the major salivary glands and ~50% in the minor glands (1-3). SACC exhibits unique characteristics compared to other tumors, such as slow but relentless growth, nerve and blood vessel invasion, and a high incidence of distant lung metastasis (4). Unfortunately, SACC has poor prognosis: survival rates after diagnosis of tumour progression are 35% at 5 years, 15% at 10 years, and 0% at 15 years (4). Late distant lung metastases are the primary cause of the low long-term survival rate in patients with SACC (5). Currently, no effective therapy is available to deter lung metastasis of SACC due to a poor understanding of the mechanisms that govern the metastasis process (6).

Epiregulin, a member of the epidermal growth factor (EGF) family of peptide growth factors, exhibits bifunctional regulatory properties: it inhibits the growth of several epithelial tumor cells and stimulates the growth of fibroblasts and various other types of cells (7). As for SACC, exogenous treatment with the recombinant human epiregulin (rhEpiregulin) protein was shown to induce epithelial-mesenchymal transition (EMT) and increase the motility of SACC cells (8, 9). However, the mechanism of the action of endogenous epiregulin on EMT and lung metastasis remains unclear.

Exosomes are small membrane vesicles (30–100 nm in diameter) containing functional biomolecules (such as proteins, lipids, RNA, and DNA) (10-14). They may diffuse to neighboring cells or be carried

via systemic transport to distant anatomic locations where they may induce signal transduction or mediate the horizontal transfer of information in specific recipient cells (15). Tumor exosomes can directly modify the intrinsic motility and invasiveness capacity of tumor cells by serving as conduit for signals that initiate EMT (15-17). Tumor exosomes can also change the cellular physiology of surrounding and distant non-tumor cells to allow dissemination and growth of cancer cells, i.e., by triggering angiogenesis and increasing vascular permeability for conditioning pre-metastatic sites in distant organs (14,18-20). To date, the different role of specific exosomes in lung metastasis remains to be elucidated. Here, we investigated the correlation between the expression of epiregulin and lung metastasis of SACC. We also examined the biological effects of epiregulin-enriched exosomes and the attendant signaling cascades they initiate.

Materials and Methods

Cell lines and transfection

The SACC-83 cell line originates from a patient's sublingual gland; SACC-LM cells with enhanced lung metastatic behavior were isolated *in vivo* following injection of SACC-83 cells into the tail vein of immunodeficient mice (21, 22). Human umbilical vein endothelial cells (HUVECs) and human pulmonary microvascular endothelial cells (HPMECs) were obtained from the PriCells (Wuhan, China) and grown in endothelial cell medium (ECM, ScienCell, USA).

The lentiviral vector pHBLV-CMV-GFP-T2A-Luc (used to construct the epiregulin-expression vector) and the pHBLV-CMVIE-RFP vector (used to construct the GLI1-expression vector) were purchased from Hanbio (Hanbio Biotechnology, China). The plasmid hU6-MCS-CMV-RFP used to construct the epiregulin-knockdown plasmid was purchased from Genechem (Genechem, China). After screening, SACC-83 cells stably overexpressing epiregulin (OE cells) and control cells (Vector cells), as well as SACC-LM cells with stably knockdowned epiregulin (siEpiregulin cells) and control cells (siControl cells) were established.

Experimental animals

The female BALB/c nude mice and NOD SCID mice (6–8 weeks old) were obtained from Vital River Laboratories (Beijing, China). The animal experiments were approved by the Peking University Institutional Animal Care and Use Committee (Permit Numbers: LA2012015; LA2015099) and were performed according to the guideline on animal experiments.

Human tissue samples and immunohistochemical analysis

All human SACC and SMG tissues used in this study were collected from patients in the Peking University School of Stomatology. A total of 107 SACC tissues (paraffin-embedded tissues) were collected from patients undergoing surgical resection from 1993 to 2008. In the 107 cases, the 72 complete follow-up records available were used for further survival analysis. In the 72 cases, 33 received radiotherapy, 1 received chemotherapy, 4 received radiotherapy and chemotherapy, and 34 received no adjuvant therapy after surgery operation. SACC specimens (60 frozen tissues) were obtained from the tumor tissue bank of the hospital. Normal SMG specimens (41 frozen tissues and 11 paraffin-embedded tissues) were collected from patients undergoing neck dissection. The use of these clinical samples was approved by the Ethics Committee of Peking University School and Hospital of Stomatology (Permit number: PKUSSIRB-201522040).

Immunohistochemistry was performed according to a standard protocol. After deparaffinization and rehydration, tissue sections were incubated in sodium citrate buffer and heated for antigen retrieval. Epiregulin (rabbit; Abcam, USA), CD31/CD34 (rabbit; Sino Biological, China), and F4/80 (rabbit; abcam) primary antibodies was applied to tissue sections overnight at 4°C. All sections were then incubated with secondary antibody for 30 minutes at room temperature. The immunoreactions were visualized and scored by two investigators blinded to the relative clinical outcome. Scores representing the percentage of positive staining tumor cells were assessed as: 0 (<5%); 1 (5–24%); 2 (25–49%); 3 (50–74%); and 4 (≥75%). The staining intensity was graded as: 0 (no staining); 1 (weak staining); 2 (moderate staining); and 3 (strong staining). The final score was determined by the ratio of positively stained tumor cells × staining intensity to produce scores of 0, 1, 2, 3, 4, 6, 8, 9, and 12. The cutoff value for low and high expression of epiregulin was identified as 6: a score greater than 6 was considered high expression, and less than or equals to 6 was considered low expression.

Metastatic burden

Image J software was used to quantify the metastatic burden within the mice lungs as previously described (23). Briefly, after hematoxylin and eosin staining, the number of pixels within the defined area of the metastatic lesions was determined as x pixels, and the total number of pixels within the field of view was determined as y pixels. The metastatic burden

within the field of view was calculated with the formula: (x pixels/y pixels) * 100. The average of 5 fields of view with 100× magnification was used to determine metastatic burden in each lung analyzed.

Western blot analysis

Western blot assay was performed according to a standard protocol. Briefly, 40 μg of protein from cells or exosomes was separated on an SDS-PAGE gel and transferred to polyvinylidenedifluoride membranes. After membranes were blocked, the following primary antibodies were used: Epiregulin (rabbit; CST), E-cadherin (rabbit; CST), Snail (rabbit; CST), Slug (rabbit; CST), GLI1 (rabbit, Abcam), N-cadherin (rabbit, CST), CD63 (rabbit, Abcam), and HSP70 (rabbit, Abcam). Equal protein sample loading was determined using anti-GAPDH/anti-β-actin (ZSGB-Bio, China) for total protein lysates. The bands were quantified using the Gel-Pro analyzer.

Microarray analysis

The SBC Human lncRNA microarray v5.0 (for mRNA/LncRNA detection) (Shanghai Biotechnology, China) was used. Altogether, 1166 differentially expressed genes were detected from OE cells and Vector cells. The recommended cut-off for the *P* value and fold change were 0.05 and 2, respectively. These genes underwent further Gene ontology (GO) analysis to identify the biological processes represented in the gene profile. The analysis was performed by Shanghai Biotechnology Corporation.

qRT-PCR

Quantification of mRNA expression was performed using FastStart Universal SYBR Green Master (ROX) reagent (Roche, USA) on an ABI 7500 Sequence Detection System. The mRNA expression of genes of interest were normalized to GAPDH, and the results were represented as fold change using ΔΔCt method with the control set as one. The sequences of the primers were shown in Supplementary Table 1.

Exosome isolation, labeling, and uptake

Exosomes were collected from supernatants of tumor cells (cultured in exosome-free medium) and isolated by ultracentrifugation and sucrose cushion (24,25). Briefly, cell supernatants were subjected to consecutive centrifugation at 300 g for 10 minutes, 2000 g for 30 minutes, and 10,000 g for 30 minutes to remove cellular debris and large vesicles. Supernatants were then passed through a Centrifugal Filter (100K, Millipore, USA) at 5,000 g for 30 minutes. The retained, concentrated supernatants were subjected to a 30% sucrose/deuterium oxide (D_2O) cushion. After gradient centrifugation at 10,0000 g for 70 minutes using an Optima L-90K Ultracentrifuge (Beckman Coulter, USA), the exosome-enriched sucrose/D_2O was resuspended in PBS for centrifugation at 5,000 g for 30 minutes in centrifugal filters. This was repeated three times to remove the sucrose/D_2O, and the retained exosomes were stored at -80°C. The protein contents of exosomes were determined using a Bradford protein assay kit (Beyotime Biotechnology, China).

Purified exosomes were labeled with a red fluorescent cell linker PKH26 (Sigma-Aldrich, USA) according to the manufacturer's protocol. Briefly, exosomes were suspended in PBS before 1 ml Diluent C was added. Meanwhile, 4 μl PKH26 was added to 1 ml Dilucent C and mixed gently with the exosome solution for 4 minutes. Then 2 ml of 0.5% BSA/PBS was added to bind excess dye. The labeled exosomes were washed with PBS at 100,000 g for 70 minutes, and exosomes were diluted in 100 μl PBS before use in the uptake assays.

Exosomes and endothelial cells were fluorescently labeled using PKH26 and Actin-Tracker Green (phalloidin-FITC, Beyotime Biotechnology, China), respectively. Cellular nuclei were stained using DAPI (ZSGB-Bio, China). Endothelial cells were incubated with labeled exosomes for 24 hours. Imaging of exosomes uptake was performed using a LSM 5 Exciter confocal laser scanning microscope (Zeiss, Germany).

Transmission electron microscopy

Transmission electron microscopy was used to identify the morphology of exosomes. Exosomes were diluted in 100 μl PBS and kept at 4°C prior to analysis. A drop of the exosome solution was loaded on a carbon-coated copper grid and left to adhere for 5 minutes. The exosome sample was then contrast stained by adding a drop of 1% phosphotungstic acid to the sample on the grid. After excess liquid was removed, the grid was positioned on a paper and left to air dry for at least 5 minutes. The preparation was examined using a JEM-1400 electron microscope (JEOL, Japan).

Cell proliferation, migration, and invasion assays

Cell viability was assessed with CCK-8 reagents (Dojindo Laboratories, Japan) according to the manufacturer's instructions. Cells were seeded in 96-well plates at 3000 cells/well in 100 μl of culture medium, and incubated with 200 μg/ml exosomes or PBS before absorbance was measured at 450 nm using an ELx808 Absorbance Microplate Reader (BioTek, USA).

For the scratch wound migration assay, HPMECs seeded in 6-well plates were cultured for 24

hours before a scratch was generated using a tip. After washing twice with PBS to remove detached cells, medium containing 50 ng/ml rhEpiregulin (Sino Biological, China) or 200 μg/ml exosomes was added. Images were captured under an Eclipse TE2000-U fluorescence microscope (Nikon, Japan). Migrated distance was quantified by the IPP software.

To analyze transwell migration/invasion, cell inserts (8.0 μm pore size, Millipore, USA) were coated without (migration) or with (invasion) matrigel (BD Bioscience, USA). Then 5×10^4 cells were seeded on the upper chamber in serum-free mediums. After 16 hours incubation with 200 μg/ml exosomes, the cells on the upper surface of the insert were swabbed, and cells in the bottom chamber were fixed with 95% ethanol, stained with 1% crystal violet, and counted under a BX51 microscope (Olympus, Japan).

Tube formation and vascular permeability assays

For the tube formation assay, 2×10^4 cells seeded on matrigel matrix-coated (Gibco, USA) wells were treated with 50 ng/ml rhEpiregulin or 200 μg/ml exosomes. After 12 hours incubation, CFSE dye (Dojindo Laboratories, Japan) was added and the optical images of the wells were acquired. Tube-like structures in each well were counted, and results represented the average number of tube-like structures in triplicate wells.

For the vascular permeability assay, endothelial cells were cultured on transwell inserts (0.4 μm pore membrane, Millipore) and allowed to form confluent monolayers (typically after 24 hours). Then complete medium containing 0.12 mg/ml FITC-labeled dextran (40 kDa) (Sigma-Aldrich) replaced the medium in the upper chamber. At each time point after rhEpiregulin or exosomes were added, 50 μl of medium in the bottom chamber was harvested, and fluorescence was measured at excitation 490 nm and emission 520 nm.

Luciferase reporter assay

Cells were seeded in 24-well plates and incubated for 24 hours. The reporter plasmid pEZX-PG04-CDH1 (GeneCopoeia,USA) and GLI1-expressing/control plasmid (Genechem, China) were transfected into SACC-83 cells using Lipofectamine 2000 reagent (Invitrogen, USA). After 36 hours, luciferase activity was measured using a Secrete-Pair™ Dual Luminescence Assay Kit (GeneCopoeia, USA) according to the manufacturer's protocol.

Quantification of VEGFA by ELISA

The secreted VEGFA in the supernatant was quantified using a human VEGF ELISA kit (Neobioscience Technology, China). Briefly, cells were seeded into 6-well plates and cultured to 70–80% confluence. The cells were then switched to fresh FBS-free medium and treated with 200 μg/ml exosomes. The number of cells in each well was counted. The supernatants (100 μl) of the samples were harvested and added to 96-well microplates. The level of VEGF-A in the 100 μl supernatant was determined at 450 nm and normalized to the cell number.

Matrigel plug assay

Matrigel matrix (500 μl; Gibco, USA) with 1×10^7 SACC-83 cells containing PBS or exosomes (100 μg) was injected subcutaneously into a flank of BALB/c female nude mice (n = 5 per group). In another matrigel plug assay, cell-free matrigel matrix (500 μl) containing Vector exosomes or OE exosomes (100 μg) was injected (n = 8 per group). On day 7, mice were sacrificed and matrigel plugs were removed and photographed to show the extent of vascularization. After weighing the matrigel plugs, immunohistochemical analysis of matrigel plugs was performed after routine paraffin embedding. Hemoglobin content of the matrigel plugs was quantified using Drabkin reagent (Sigma-Aldrich, USA).

Vascular permeability assay

Lung microvasculature permeability was determined by the Evans Blue (EB, Sigma-Aldrich, USA) extravasation technique. After 5 days of daily intravenously injection of exosomes (70 μg), the BALB/c female nude mice were injected with EB reagent (20 mg/ml). After 3 hours, pulmonary microvasculature was flushed via transcardial perfusion with PBS under physiologic pressure, then the lungs were harvested, rinsed, photographed, and frozen in liquid nitrogen. The frozen lungs were later homogenized in formamide and incubated at 60°C for 16 hours. The absorbance of the supernatant was measured by spectrophotometry at 620 nm and used to determine the amount of EB.

Mouse model of lung metastasis

To identify the role of epiregulin in SACC lung metastasis *in vivo*, 1×10^6 OE cells or Vector cells were injected into the tail veins of NOD SCID mice (n = 6 per group). After 8 weeks, the bioluminescence of mice was measured using the IVIS Imaging System (Caliper Life Sciences, USA) to monitor the lung metastasis of tumor cells. The mice were then sacrificed and their lungs collected for HE staining.

To observe the effect of exosomes on lung metastasis, PBS (100 μl) with or without exosomes (70 μg) was injected intravenously daily into NOD SCID

(n = 6 per group) mice for 5 days. On day 5, mice were received an intravenous injection of 1 × 10^6 SACC-83 cells. After 8 weeks, the mice were sacrificed and their lungs were collected for H&E analysis.

To compare the contribution of different exosomes to lung metastasis, PBS (100 µl) with OE exosomes or vector exosomes (70 µg) was injected intravenously daily into NOD SCID (n = 7 per group) mice for 5 days. On day 5, mice were given an intravenous injection of 1 × 10^6 SACC-83 Vector cells. After 8 weeks, the bioluminescence was detected. Then the mice were sacrificed and their lungs were collected for immunofluorescence analysis using a LSM 5 Exciter confocal laser scanning microscope (Zeiss, Germany).

Flow cytometric analysis

Exosomes (10 µg) were incubated with 5 µl of 4 µm latex-beads (Thermo Fisher Scientific, USA) for 30 minutes at 4°C. The mixture was then resuspended and incubated in 400 µl PBS (5% BSA) for 30 minutes, and the exosomes were conjugated with the latex beads. After being washed twice and resuspended in 50 µl PBS and 5% BSA, the exosome-conjugated beads were incubated with CD63 (Abcam, USA) or epiregulin (CST, USA; or Absin Bioscience, China) primary antibody, and then Alexa Fluor 488-labeled secondary antibody (Beyotime Biotechnology, China) in sequence. Finally, the sample was resuspended in 500 µl PBS. Primary antibody-free incubation samples were used as controls.

Single cell suspensions derived from SACC-83 cells were washed in PBS, fixed in 4% (v/v) paraformaldehyde, blocked with 5% BSA in PBS for 30 minutes at 4°C, and then rinsed. Cells were then incubated with epiregulin primary antibody (CST, USA; or Absin Bioscience, China) for 1 hour at 4°C, and then incubated with Alexa Fluor 488-labeled secondary antibody (Beyotime Biotechnology, China).

NOD SCID mice (n = 8 per group) were injected intravenously daily for 5 days with 70 µg of Vector/OE exosomes in 100 µl PBS. On day 5, mice were sacrificed and their lungs were collected for qRT-PCR and murine lung endothelial cells sorting. Endothelial cell sorting and detection of VEGFR1 were performed as previously described (26). Briefly, lung cells were gently dispersed in collagenase (Sigma, USA) with the MACS Dissociator (Miltenyi Biotec, Germany). Endothelial cells were isolated using CD146 microbeads (Miltenyi Biotec, Germany) according to the manufacturer's protocol. After identification, endothelial cells were detected with the anti-VEGFR1 (R&D Systems, USA) antibody.

Statistical analysis

All statistical analyses were carried out with SPSS Version 19.0 (IBM). All *in vitro* experiments were confirmed in at least three independent experiments, and the data from one representative experiment were shown. All numerical data represent mean ± standard deviation (SD), unless otherwise noted. Log-rank test are used for Kaplan-Meier analyses. Data were statistically analyzed by 2-tailed t-test or ANOVA, unless otherwise indicated. *P* values less than 0.05 were considered statistically significant.

Results

Epiregulin is overexpressed in SACC tissue samples and is associated with poor prognosis

We observed higher mRNA expression of epiregulin in SACC than SMG in 60 frozen SACC and 41 frozen submandibular gland (SMG) tissue samples (Figure 1A). The finding was further validated via immunohistochemical analysis of 107 SACC and 11 SMG tissues samples (Figure 1B and Table 1). We then stratified SACC patients according to epiregulin expression. High epiregulin levels were observed in SACC patients with a large tumor size (≥ 4 cm) and higher clinical stage (stage III/IV) ($P < 0.0001$) (data not shown).

Table 1. Immunohistochemical analysis of epiregulin protein levels in 107 SACC tumors and 11 normal submandibular gland (SMG) tissues.

IHC	Epiregulin		
	Low	High	Total
Tissue			
SMG	11 (100%)	0 (0%)	11
SACC	49 (46%)	58 (54%)	107
Total	60	58	118

Of the tissue samples collected from 107 SACC patients, 72 cases with complete outcome data were further evaluated. Kaplan-Meier survival analysis showed that the additional adjuvant treatment after surgery could not increase the cumulative survival and metastasis-free survival in 72 SACC patients (data not shown), and therefore the effects of radiotherapy and chemotherapy were not taken into consideration. We found high epiregulin expression was associated with a high incidence of lung metastasis ($P = 0.002$) and a high rate of local recurrence ($P = 0.044$) (Table 2). Moreover, Kaplan-Meier survival analysis showed that high epiregulin levels in SACC patients were significantly correlated with poor prognosis in terms of both cumulative survival (Figure 1C) and metastasis-free survival (Figure 1D).

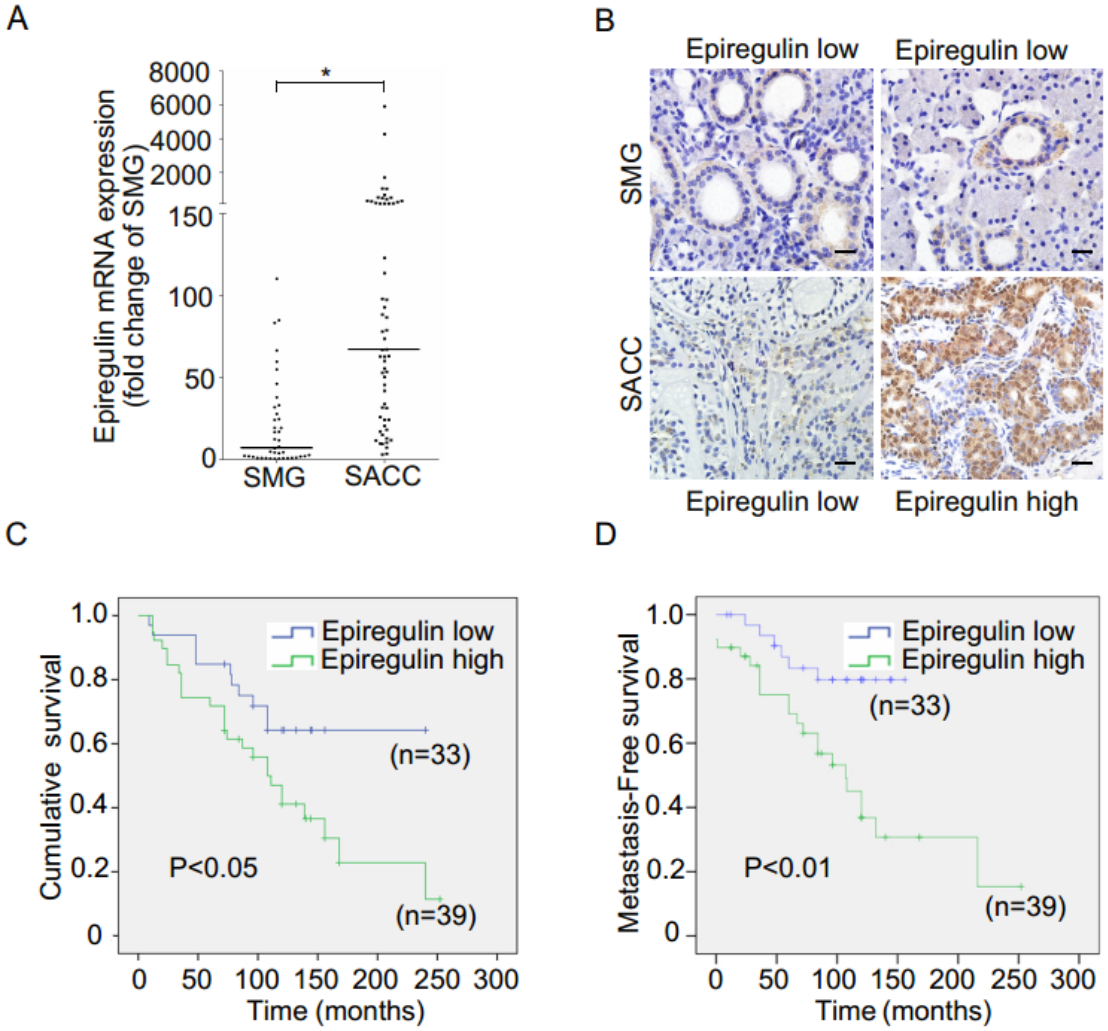

Figure 1. Expression of epiregulin is upregulated in SACC and is correlated with poor clinical outcome. (A) Real-time PCR analysis of the expression of epiregulin in 60 human SACC tissue samples compared with 41 normal SMG tissue samples. *P < 0.05, Mann-Whitney U rank sum test. (B) Immunohistochemical analysis of epiregulin expression in 107 human SACC tissue samples and 11 normal SMG tissue samples, Scale bar = 20 μm. (C, D) Kaplan-Meier curves for cumulative and metastasis-free survival time. A total of 72 SACC patients were classified into high- or low-epiregulin groups, according to their immunohistochemistry staining score.

Epiregulin induces a prometastatic phenotype in SACC cells in vitro and promotes lung metastasis in vivo

To investigate the biological role of epiregulin in SACC cells, we first studied the expression of epiregulin in parental SACC-83 cells and in a subset of SACC cells that exhibit high lung metastasis (SACC-LM). Epiregulin was highly expressed in SACC-LM cells compared with the parental SACC-83 cells (Figure 2A). Meanwhile, we generated OE cells and Vector cells (Figure 2B). We also established SACC-LM cells with stably knockdowned epiregulin (siEpiregulin cells) and control cells (siControl cells) (Figure 2C). Overexpression of epiregulin in OE cells induced transformed morphological characteristics of EMT, identified by a spindle-like morphology and decreased cell-cell adhesion. In contrast, siEpiregulin cells exhibited shrinkage morphology (Supplementary Figure 1A). Migration and invasion activity was also significantly increased in OE cells and decreased in siEpiregulin cells (Supplementary Figure 1, B and C). Moreover, OE cells exhibited a markedly increased metastatic potential in the mouse models (Figure 2, D and E).

Next we showed that GLI1 and E-cadherin are involved in the EMT induced by epiregulin. Overexpression of epiregulin in SACC-83 cells decreased the expression of GLI1 and E-cadherin and increased N-cadherin expression, while stable knockdown of epiregulin in SACC-LM cells significantly increased the expression of GLI1 and E-cadherin and decreased the N-cadherin expression (Figure 2F). As further evidence, transfection of the GLI1-expressing lentiviral vector in OE cells rescued the expression of E-cadherin and decreased their

migratory and invasive ability (Figure 2, G-I). Moreover, enhanced expression of GLI1 significantly elevated the promoter activity of E-cadherin in SACC-83 cells (Figure 2J).

Table 2. Correlation between the clinicopathological variables and expression of epiregulin in patients with SACC.

Variables	Epiregulin expression				
	Total	Low	High	χ^2	*P*-value
	N	N	N		
Age (y)					
<42	32	14	18	0.101	0.751
≧42	40	19	21		
Gender					
Male	21	7	14	1.866	0.172
Female	51	26	25		
Tumor size					
<4cm	47	29	18	13.730	0.000
≧4cm	25	4	21		
Clinical stage					
I/II	36	25	11	16.168	0.000
III/IV	36	8	28		
Site					
Major salivary gland	20	9	11	0.008	0.930
Minor salivary gland	52	24	28		
Histological subtype					
Cribriform/Tubular	61	26	35	1.658	0.198
Solid	11	7	4		
Lymph node metastasis					
Absent	64	29	35	0.000	1.000
Present	8	4	4		
Perineural invasion					
Absent	32	17	15	1.234	0.267
Present	40	16	24		
Lung metastasis					
Absent	43	26	17	9.206	0.002
Present	29	7	22		
Local regional recurrence					
Absent	26	16	10	4.043	0.044
Present	46	17	29		

Epiregulin increases angiogenesis and permeability of endothelial cells

Heatmap and GO enrichment analysis was conducted on a microarray of the OE and Vector cells to identify the main biological processes in which the differentially expressed genes were involved. In addition to EMT, heatmap analysis (Supplementary Figure 2) and most GO terms were related to angiogenesis (Figure 3A). As supporting evidence, we showed that treatment with rhEpiregulin increased capillary formation, migration, and permeability of HPMECs (Figure 3, B–D). The expression of VEGFA, FGF-2, and IL-8 was significantly increased in OE cells, and decreased in siEpiregulin (Figure 3, E and F). Treatment with rhEpiregulin increased the angiogenesis-related molecules expression in HPMECs (Figure 3G). Moreover, epiregulin expression was positively correlated with VEGFA, FGF-2, IL-8, VEGFR1/2 and FGFR2 expression in the 60 available SACC patient specimens (Figure 3H).

Exosomes enhance tumor angiogenesis and vascular permeability and promote metastasis of SACC to the lung

Exosomes derived from SACC-83 cells contribute to the highly metastatic characteristics of SACC-83 cells (Supplementary Figure 3). To examine whether SACC-83-derived exosomes could be transferred to endothelial cells, HPMECs were cultured with PKH26-labeled exosomes, and the uptake of exosomes was visualized using confocal microscopy (Figure 4A). The exosomes significantly enhanced invasion of HPMECs, as well as endothelial tube formation, and endothelial permeability (Figure 4, B–D). These angiogenic functions of exosomes appear to be mediated by increasing the expression of the angiogenic factors, VEGFA, FGF-2, and IL-8 in HPMECs (Figure 4E).

Next, the effect of exosomes on tumor blood vessel development was evaluated by subcutaneously injecting exosomes mixed with SACC-83 cells in a matrigel matrix into mice. Mouse CD31-stained tumor sections demonstrated that treatment with exosomes increased the formation of $CD31^+$ blood vessels *in vivo* (Figure 4F). Interestingly, the addition of exosomes also increased the presence of macrophage cells in the matrigel plugs, as shown with F4/80 antibody staining (Supplementary Figure 4). We also carried out permeability assays by intravenously injecting exosomes (or PBS) into nude mice, followed by an intravenous EB injection. Treatment with exosomes significantly increased lung vascular leakage of EB (Figure 4G). In addition, exosome treatment significantly increased the number of metastatic nodules in an *in vivo* mouse lung metastasis model (Figure 4H). F4/80 antibody staining also showed exosomes injection increased the presence of macrophage cells in the lung pre-metastatic niche (Supplementary Figure 5A).

Epiregulin-enriched exosomes enhance angiogenic activity of endothelial cells in vitro

Electron microscopy showed that the exosomes derived from both OEs and Vector cells were quasi-circular and smaller than 100 nm (Figure 5A). Western blot demonstrated that increased expression of epiregulin was observed in OE exosomes (Figure 5B). Flow cytometry indicated no obvious expression of epiregulin in the exosome membrane, while it was enriched in the plasma membrane surface of SACC-83 cells. However, abundant CD63 protein was abundant in the surface of exosomes (Figure 5C). It was also observed that endothelial cells internalized PKH26-labeled exosomes (Figure 5D).

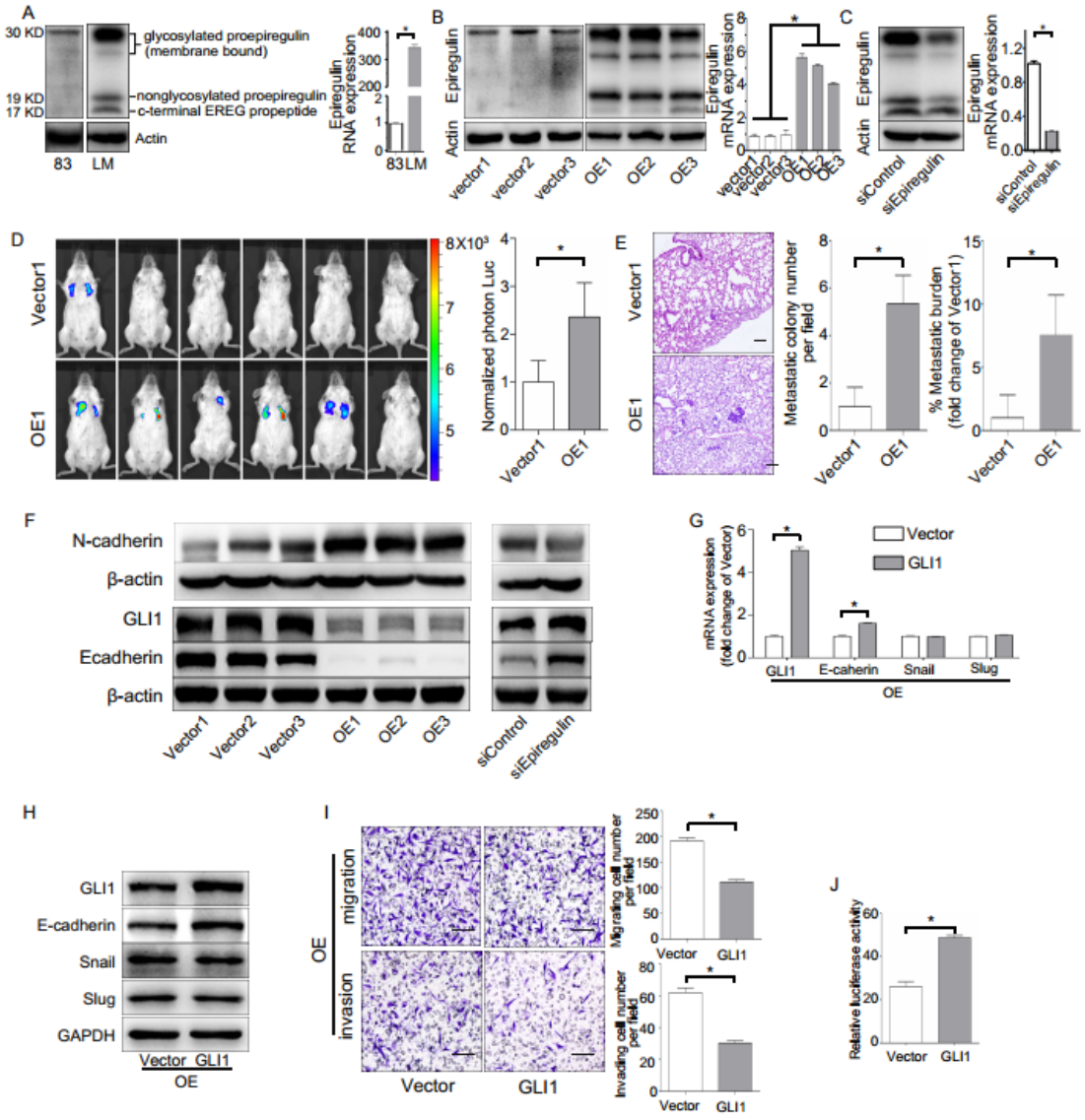

Figure 2. Effect of epiregulin on migration, invasion, and lung metastasis of SACC cells. (A) Protein expression of epiregulin in SACC-83 cells and SACC-LM cells. Actin was used as a control. (B) Protein and mRNA expression of epiregulin in SACC-83 cells stably transfected with the control vector (Vector) or the epiregulin expression vector (OE). (C) Protein and mRNA expression of epiregulin in SACC-LM cells stably transfected with control siRNA (siControl) or epiregulin siRNA (siEpiregulin). (D) Visualization of lung metastasis after intravenous injection of Vector cells or OE cells in NOD SCID mice. Representative images of bioluminescence signals and normalized photon flux are shown. (E) Representative images and quantification of metastatic tumor nodules and metastatic burden in the lung section of NOD SCID mice intravenously injected with Vector cells or OE cells. Scale bar = 100 μm. (F) Western blot analysis of N-cadherin, GLI1 and E-cadherin expression levels in differentially epiregulin-expressing SACC cells. β-actin was used as a control. (G, H) mRNA and protein expression of GLI1, E-cadherin, Snail, and Slug in OE cells transiently overexpressing GLI1 plasmid or Vector plasmid. GADPH was used as a control. (I) Migration and invasion assays of OE cells transiently overexpressing GLI1 or the Vector plasmid. Scale bar = 100 μm. (J) Dual luciferase assay showing relative E-cadherin promoter luciferase reporter gene activity in SACC-83 cells incubated with the GLI1 plasmid or Vector plasmid. All data are expressed as mean ± SD, **P* < 0.05.

OE exosomes increased the expression of epiregulin and the number of tube-like structures in the endothelial cells (Figure 5, E and F). SiEpiregulin exosomes decreased the formation of tube-like structures (Figure 5G). Moreover, OE exosomes increased the mRNA levels of VEGFA, FGF-2, and IL-8 in HPMECs (Figure 5H). ELISA assay also indicated that OE exosome-treated HPMECs released more VEGFA protein at 15, 30, and 60 minutes than Vector exosome-treated cells (Figure 5I).

Epiregulin-enriched exosomes promote lung pre-metastatic niche formation and metastasis

Gross observation, CD31/CD34 immunohistochemical analysis, and quantification of hemoglobin (Figure 6, A-C) indicated that implantation with OE exosomes induced more capillaries. Implantation with OE exosomes also increased the leakage of EB in mice lung (Figure 6D). Moreover, intravenous injection of OE exosomes in immunodeficient (NOD SCID) mice significantly increased the lung metastases of SACC (Figure 6E). OE exosomes

treatment also increased the presence of macrophage cells in the in vivo mouse lung metastasis model (Supplementary Figure 5B).

Finally, we evaluated whether epiregulin-enriched OE exosomes promoted the formation of a pre-metastatic niche in mice lungs compared with Vector exosomes. Our flow cytometric analysis showed that VEGFR1 expression, which has previously been shown to be involved in the generation of lung pre-metastatic niche (26-29), was significantly increased in CD146⁺-sorted lung endothelial cells following stimulation with OE exosomes compared with Vector exosomes (Figure 6F). Meanwhile, although there were no significant differences in mRNA expression in the total lung tissue between the two treatment groups, OE exosomes significantly enhanced the mRNA expression of VEGFA, FGF-2, and IL-8 in the CD146⁺-sorted lung endothelial cells (Figure 6G).

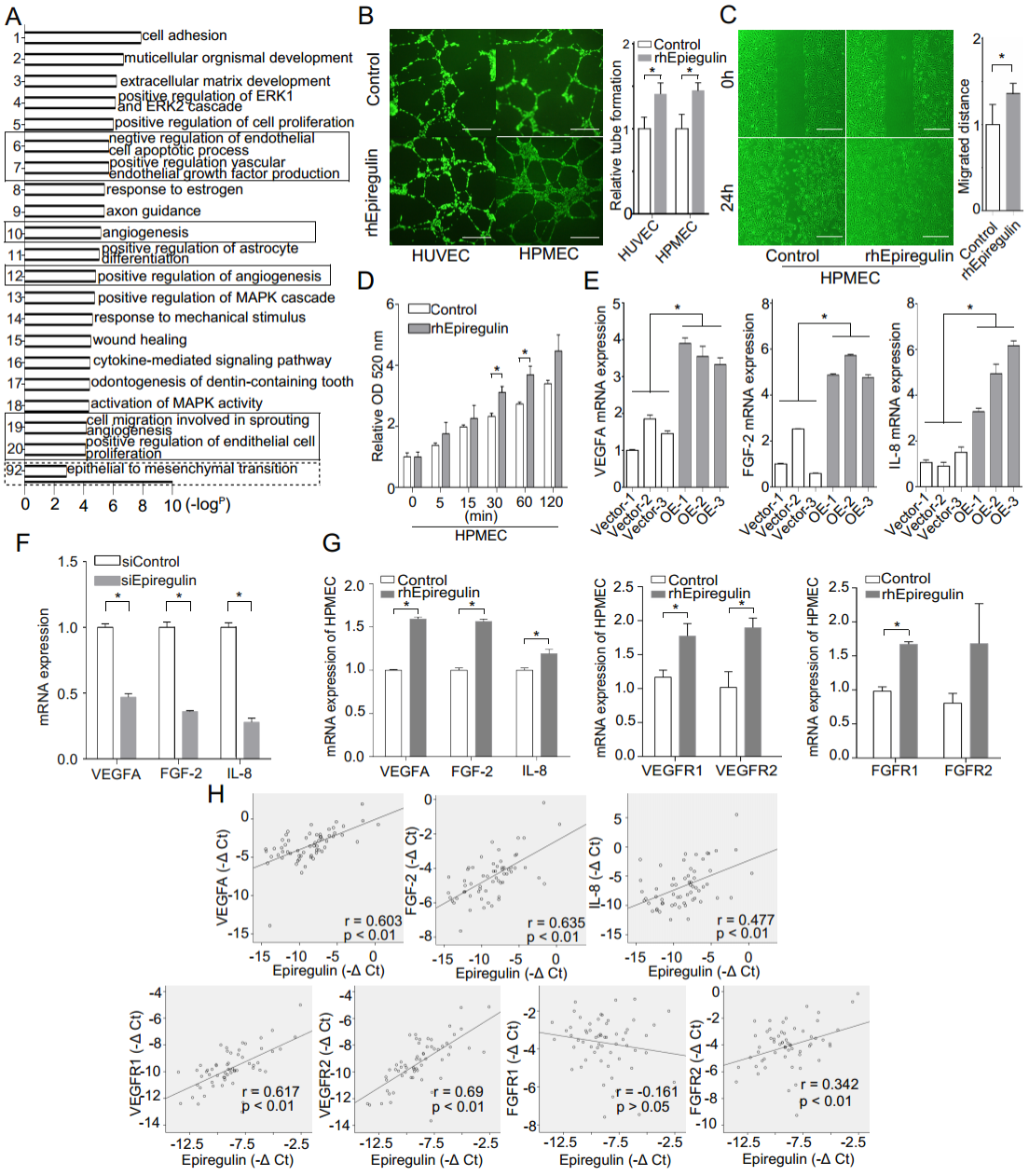

Figure 3. Epiregulin is involved in the angiogenesis and permeability of endothelial cells. (A) Gene ontology (GO) analysis of differentially expressed mRNAs in Vector cells and OE cells. GO annotation of biological process with the top 20 enrichment scores cover the domains of pro-angiogenic process (solid line frame), as well as the EMT process (dotted line frame). (B) Representative images and quantification of tube formation of endothelial cells 12 hours after incubation with HUVECs or HPMECs with 50 ng/ml epiregulin. Scale bar = 500 μm. (C) Representative images of the migration of HPMECs cultured with 50 ng/ml epiregulin in a wound healing assay, and quantification of the scratch closure 16 hours after generating the scratch. Scale bar = 500 μm. (D) Permeability assay in HPMECs exposed to 20 ng/ml epiregulin. Results are expressed as fold change relative to the control group. (E, F) Real-time PCR of relative VEGFA, FGF-2, and IL-8 mRNA expression levels in OE/Vector and siEpiregulin/siControl cells. (G) rhEpiregulin increased the expression of VEGFA, FGF-2, IL-8, VEGFR1/2, and FGFR1/2 mRNA in HPMECs. (H) Correlation of epiregulin levels with VEGFA, FGF-2, IL-8, VEGFR1/2, and FGFR1/2 mRNA levels in SACC tissues (n = 60). Pearson correlation coefficient with the respective significance is indicated. All data are expressed as mean ± SD, $^*P < 0.05$.

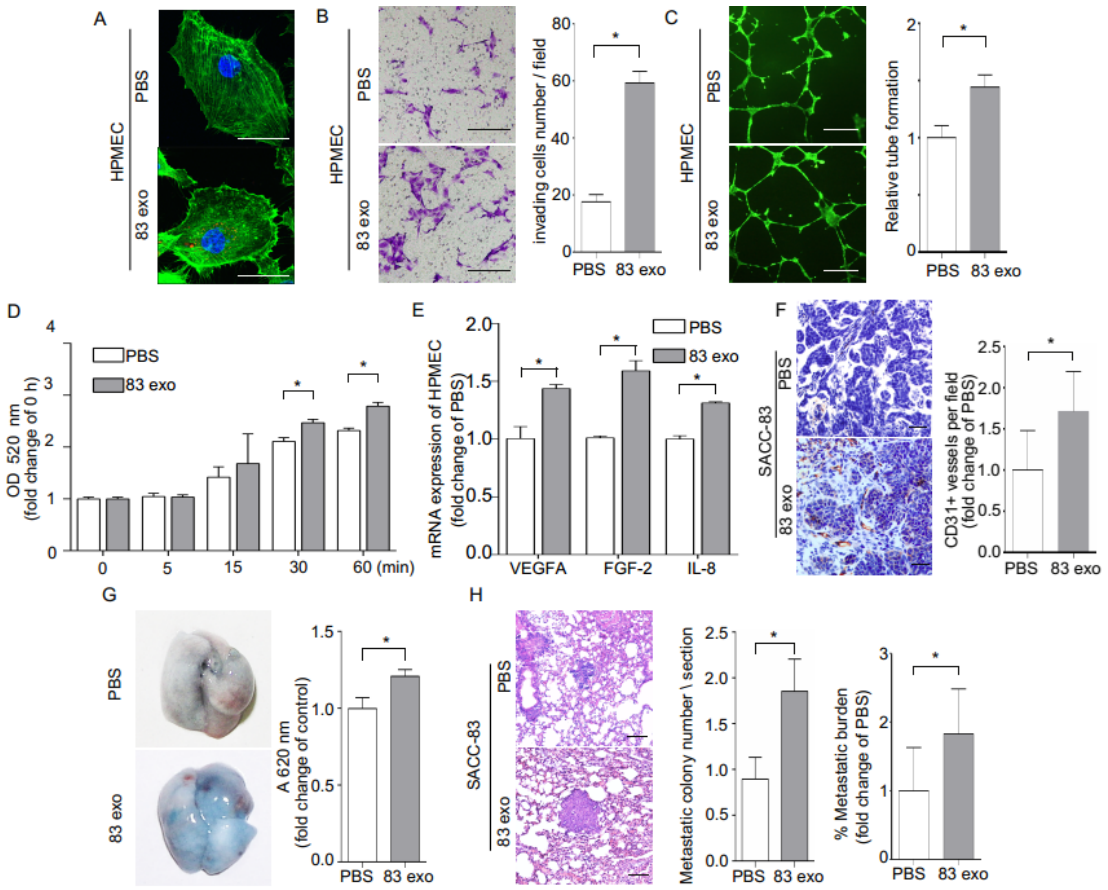

Figure 4. Exosomes derived from SACC-83 cells (83 exo) promote angiogenesis and vascular permeability, and increase the lung metastasis of SACC-83 cells. (A) The uptake of PKH26-labeled exosomes (red) by HPMECs, detected with fluorescence confocal microscopy. Scale bar = 10 μm. (B) Invasion assay for HPMECs after incubation with or without 83 exo. Scale bar = 200 μm. (C) Tube formation assay for HPMECs after incubation with or without 83 exo. Scale bar = 500 μm. (D) Permeability assay for HPMECs after incubation with or without 83 exo. (E) Real-time PCR analysis of relative VEGFA, FGF-2, and IL-8 mRNA expression levels in HPMECs after treatment with or without 83 exo. (F) Immunohistochemical analysis of CD31 in SACC-83 tumor grafts in nude mice after incubation with or without 83 exo (n = 5 per group). Scale bar = 50 μm. (G) Representative images of Evans Blue (EB) leakage in the lungs of nude mice 5 days after stimulation with or without 83 exo. (n = 5 per group). (H) Representative immunohistochemical images of experimental lung metastases in NOD SCID mice pre-stimulated with or without 83 exo (n = 6 per group). Scale bar = 100 μm. Quantification of lung metastatic tumor nodules and metastatic burden assessed by H&E staining on lung non-consecutive sections. The data are expressed as mean ± SD except for (H), which is presented as mean ± SEM. *$P < 0.05$.

Discussion

Liu *et al.* (9) indicated that the high epiregulin levels had a significantly shorter median overall survival in patients with head and neck cancer. In this study, we first show the positive relationship between the expression of epiregulin and metastasis to lung in patients. High tissue levels of epiregulin in primary tumor is a predictor of liver metastasis and a poor prognosis in patients with colorectal cancer; therefore, epiregulin appeared to be a useful prognostic marker in KRAS wild-type patients who never received anti-EGFR therapy (30-32). Patients with metastatic colorectal cancer that have high gene expression levels of epiregulin and amphiregulin and wild-type K-ras are more likely to have disease control on cetuximab treatment (33). High epiregulin mRNA is independent favorable prognostic biomarker in RAS-wild type metastatic colorectal cancer patients receivng anti-EGFR therapy (34). Our data also showed that high epiregulin expression in SACC was significantly correlated with poor prognosis in terms of both cumulative survival and metastasis-free survival. Although we were not able to demonstrate that epiregulin was an independent prognostic factor for poor outcome in SACC patients, the identified marker might be developed further to be a therapeutic target in SACC.

Our previous study showed that EMT is involved in metastasis of SACC to the lung (35, 36). While EMT is a critical event for tumor metastasis, its regulatory mechanisms are not completely clear. We found that Gli1, a key transcription activator of the Sonic Hedgehog (Shh) signaling pathway, is closely linked to the epiregulin-induced EMT in SACC. Furthermore, Gli1 levels were positively correlated with E-cadherin expression in epiregulin-induced EMT. Studies of the relationship between the Shh pathway and EMT have recently emerged, but they remain controversial. Most studies, such as Inaguma

et al. (37), suggest that Gli1 facilitates cancer cell migration and invasion through negative regulation of E-cadherin in melanoma and pancreatic cancers. On the contrary, Joost et al. (38) proposed that inhibition of Gli1 promoted EMT in pancreatic cancers and that Gli1 is positively related to E-cadherin expression. Our results show that upregulation of Gli1 rescues E-cadherin expression in epiregulin-induced EMT, which in turn, decreases the migration and invasion of epiregulin-overexpressing SACC cells.

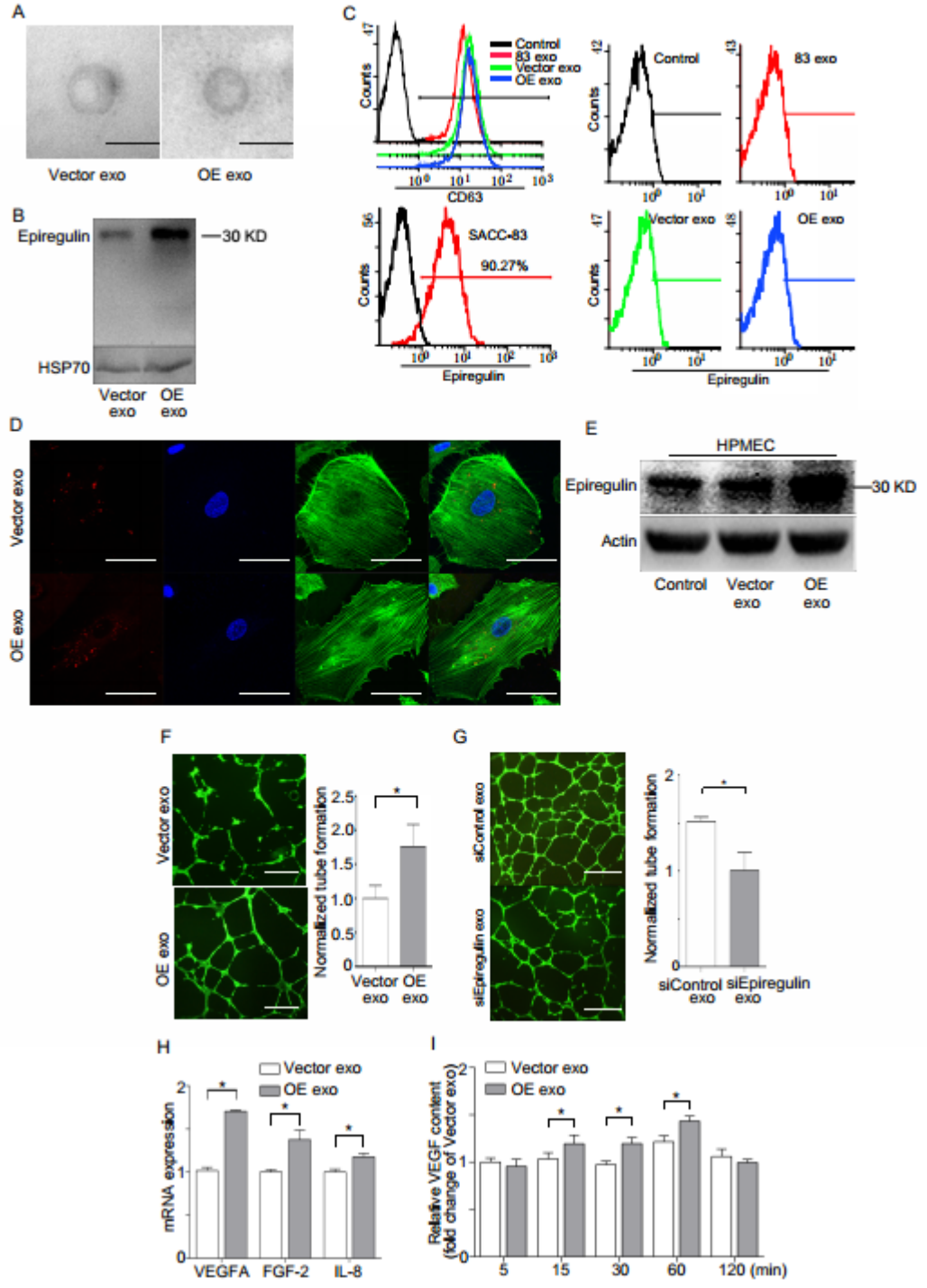

Figure 5. Epiregulin-enriched exosomes derived from SACC-83 cells stably overexpressing epiregulin (OE exo) enhance the angiogenic activity of endothelial cells *in vitro*. (A) Electron microscopy images of Vector exosomes and OE exosomes (scale bar = 100 nm). (B) Western blot assay for epiregulin and HSP70 (exosomal marker) expression in Vector exosomes and OE exosomes. (C) Flow cytometric analysis of epiregulin expression in Vector exosomes and OE exosomes. (D) Confocal images of HPMECs incubated with PKH26-labeled (red) Vector exosomes or OE exosomes for 24 hours. Scale bar = 10 μm. (E) Western blot assay for epiregulin expression in HPMECs incubated with Vector exosomes or OE exosomes. (F) Representative images of tube formation of HPMECs 12 hours after incubation with Vector exosomes or OE exosomes. Scale bar = 500 μm. (G) Real-time PCR analysis of relative VEGFA, FGF-2, and IL-8 mRNA expression in HPMECs after treatment with Vector exosomes or OE exosomes. (H) ELISA analysis of VEGF levels in the conditioned medium of HPMECs after the addition of indicated exosomes. All data are expressed as mean ± SD, **P* < 0.05.

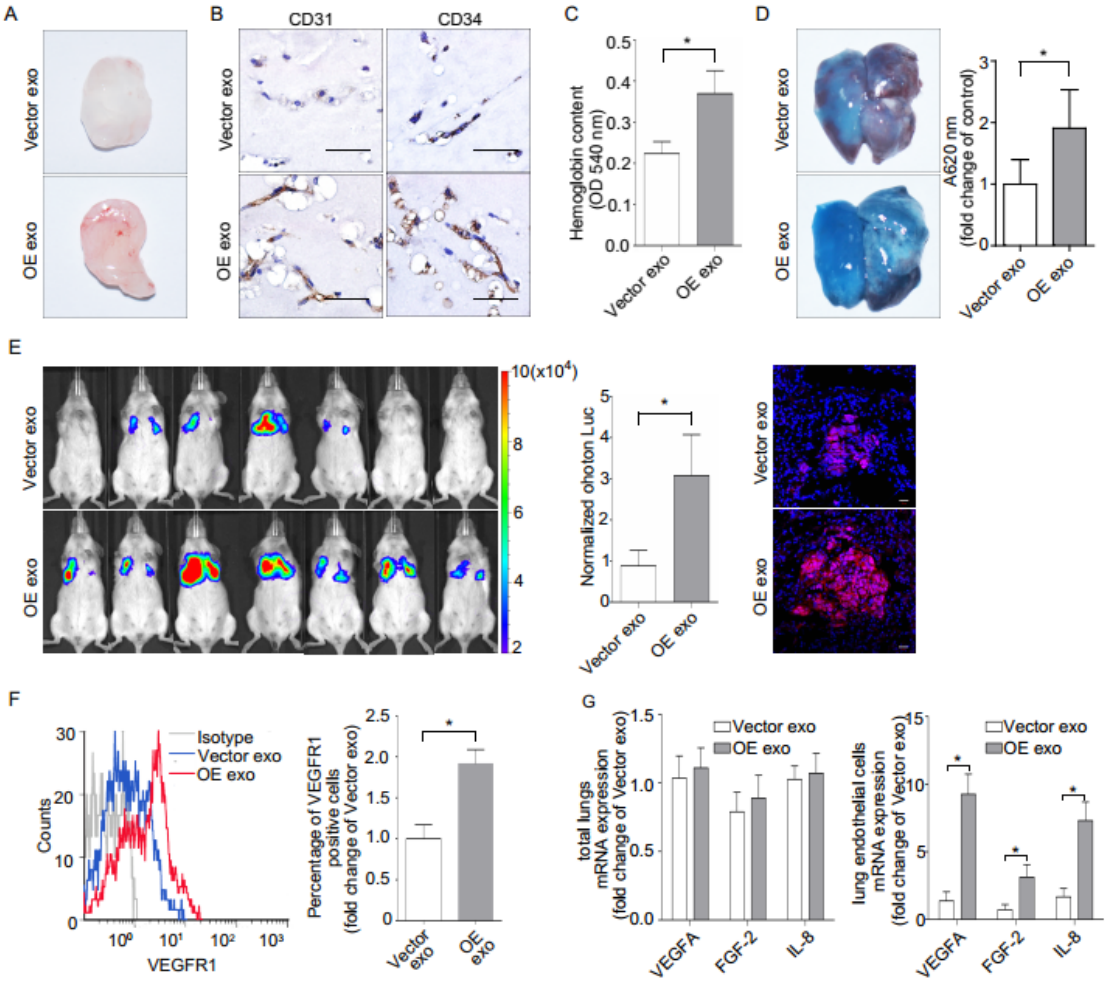

Figure 6. Effect of epiregulin-enriched exosomes (OE exo) on angiogenesis, permeability of endothelial cells, and lung metastasis *in vivo*. (A, B) Representative images of the general observation and the CD31/CD34 immunohistochemical staining of the matrigel plugs (n = 8 per group; scale bar = 50 μm). (C) The hemoglobin content of the matrigel plugs (n = 8 per group). Data are shown as mean ± SEM. (D) Representative images and quantification of Evans Blue (EB) leakage in the lung in nude mice 5 days after stimulation with the indicated exosomes (n = 3 per group). Data are shown as mean ± SEM. (E) The formation of lung metastasis in mice after stimulation with Vector exosomes or OE exosomes, as represented by bioluminescence signals (left) and normalized photon flux (middle). Representative immunofluorescence images of HLA-A-labeled Vector cells (red) in frozen tumor-bearing lung sections (right). Scale bar = 20 μm. (F) Flow cytometric analysis of VEGFR1 expression in CD146$^+$-sorted lung endothelial cells from mice. Relative percentage of positive cells are shown. (G) Real-time PCR analysis of VEGFA, IL-8, and FGF-2 expression in the total lungs from mice and in the CD146$^+$ sorted murine endothelial cells obtained from treated mice (n = 8 per group). The data are expressed as mean ± SD except otherwise stated, *$P < 0.05$.

Epiregulin has previously been implicated in inflammation, wound-healing, normal physiology, and vascular remodeling (39-41). Using microarray analysis, we showed that upregulation of epiregulin increased the expression of angiogenic and vascular remodeling related factors in SACC cells. In addition, we found a positive correlation between epiregulin and important angiogenic factors, such as VEGFA, bFGF, and IL-8. During the metastasis process of malignant tumor cells, the increasement of vascular permeability has been believed as an early event (42). Furthermore, we found that epiregulin increases vascular endothelial cell angiogenesis and permeability *in vitro* and promotes lung metastasis of SACC cells *in vivo*.

Based on our findings in two adenoid cystic carcinoma cell lines SACC-83 and SACC-LM, and those in the literature, we propose the term 'exosomecrine' be used to denote intercellular signaling transduction by exosome-mediated transfer of material. The transfer of materials between cells has been identified via autocrine, paracrine, and juxtacrine mechanisms (20, 43). The nature of exosome mediation, which enables distant communication, distinguishes exosomecrine from the autocrine, paracrine, and juxtacrine. Recently, exosomes were identified as a major cellular source of protein in the tumor microenvironment, and exosomes derived from tumor cells were shown to reprogram the tumor microenvironment to be tumor promoting (18, 44, 45). Specifically, a previous study demonstrated that amphiregulin, an EGFR ligand, was released as full-length, exosome-surface ligand (which is different from the cleaved form used in

autocrine/paracrine processes) and can result in increased tumor invasive ability (46). Our current study shows that epiregulin secreted in an exosomecrine manner is also a full-length uncleaved ligand, but not at the surface of exosomes, indicating that EGFR ligands are secreted in various forms. Given that epiregulin is a ligand for EGF family receptors, this implies epiregulin may have independent signaling functions in the cytoplasm after internalization via exosomes.

We showed that epiregulin-enriched exosomes were able to significantly enhance lung metastasis when injected prior to SACC cells. Epiregulin-enriched exosomes enhanced the expression of VEGF, FGF-2, and IL-8 in both SACC and lung vascular endothelial cells *in vitro* and *in vivo*, thus contributing to angiogenesis. Moreover, epiregulin-enriched exosomes elevated the expression of VEGFR1 in $CD146^{+}$-sorted lung endothelial cells, and VEGFR1 is known to be involved in generating the pre-metastatic niche in lung (26-29). Our results suggest that epiregulin-enriched exosomes can elicit a receptive pre-metastatic microenvironment by remodeling the lung vascular endothelial cells, thus coordinating the metastatic diffusion of SACC cells, as summarized in Figure 7.

It is important to note that as exosomes can transport a variety of molecules (such as protein, microRNA, LncRNA, DNA), we could not posit a precise causal relationship solely between the epiregulin found within exosomes and the changes in the surrounding tumor or distant pre-metastatic lung microenvironments. However, our findings demonstrate that epiregulin-enriched exosomes derived from epiregulin-overexpressing SACC cells promote lung metastasis more effectively, by influencing both SACC cells and endothelial cells, with the upregulation of VEGFA, bFGF, and IL-8.

In summary, our findings indicate that epiregulin in SACC is a critical oncoprotein that facilitates metastasis. Epiregulin acts via exosomes to facilitate metastasis not only by directly affecting host tumor cells, but also influencing the surrounding tumor cells and distant lung endothelial cells. Thus, epiregulin and epiregulin-containing exosomes may represent an important therapeutic target for controlling lung metastasis in patients with SACC.

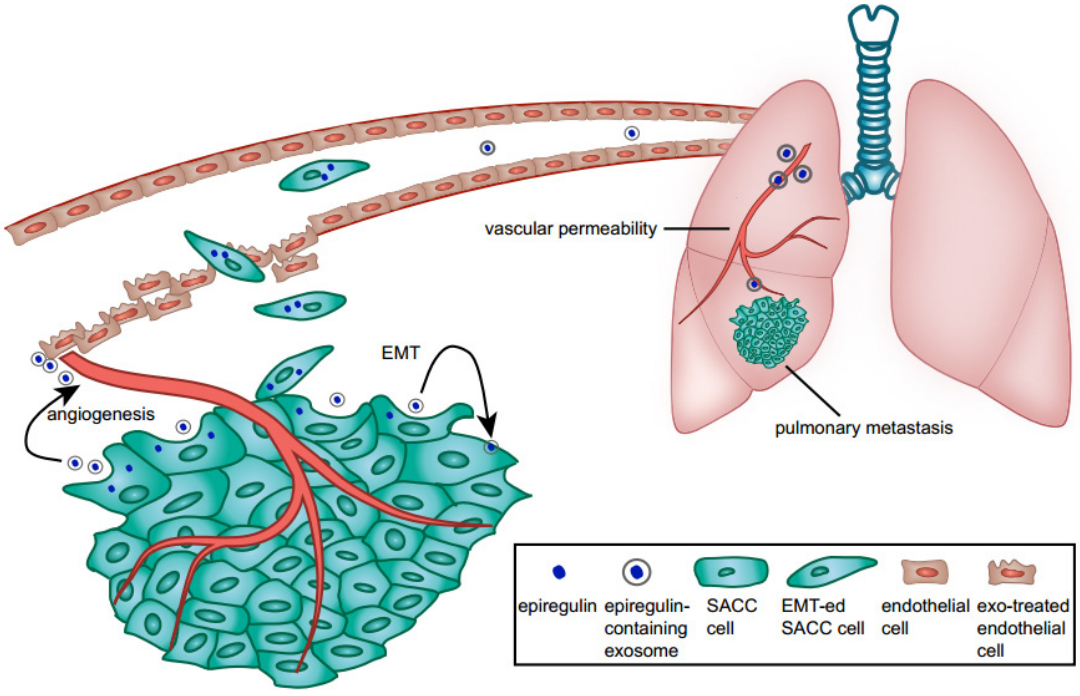

Figure 7. Schematic diagram of the role of epiregulin and epiregulin-enriched exosomes in the initiation of pre-metastatic niche formation and metastasis.

Acknowledgement

This study was supported by the National Natural Science Foundation of China (No. 81272967 and 81272966).

Supplementary Material

Supplementary figures and tables.
http://www.thno.org/v07p3700s1.pdf

Competing Interests

The authors have declared that no competing interest exists.

References

1. Renehan A, Gleave EN, Hancock BD, Smith P, McGurk M. Long-term follow-up of over 1000 patients with salivary gland tumours treated in a single centre. Br J Surg 1996;83:1750-4
2. Anderson JN, Jr., Beenken SW, Crowe R, Soong SJ, Peters G, Maddox WA, *et al.* Prognostic factors in minor salivary gland cancer. Head Neck 1995;17:480-6
3. Laurie SA, Ho AL, Fury MG, Sherman E, Pfister DG. Systemic therapy in the management of metastatic or locally recurrent adenoid cystic carcinoma of the salivary glands: a systematic review. The lancet oncology 2011;12:815-24
4. Kokemueller H, Eckardt A, Brachvogel P, Hausamen JE. Adenoid cystic carcinoma of the head and neck--a 20 years experience. Int J Oral Maxillofac Surg 2004;33:25-31
5. van der Wal JE, Becking AG, Snow GB, van der Waal I. Distant metastases of adenoid cystic carcinoma of the salivary glands and the value of diagnostic examinations during follow-up. Head Neck 2002;24:779-83
6. Huang Y, Yu T, Fu X, Chen J, Liu Y, Li C, *et al.* EGFR inhibition prevents in vitro tumor growth of salivary adenoid cystic carcinoma. BMC cell biology 2013;14:13
7. Toyoda H, Komurasaki T, Uchida D, Takayama Y, Isobe T, Okuyama T, *et al.* Epiregulin. A novel epidermal growth factor with mitogenic activity for rat primary hepatocytes. J Biol Chem 1995;270:7495-500
8. Hu K, Li SL, Gan YH, Wang CY, Yu GY. Epiregulin promotes migration and invasion of salivary adenoid cystic carcinoma cell line SACC-83 through activation of ERK and Akt. Oral Oncol 2009;45:156-63
9. Liu S, Ye D, Xu D, Liao Y, Zhang L, Liu L, *et al.* Autocrine epiregulin activates EGFR pathway for lung metastasis via EMT in salivary adenoid cystic carcinoma. Oncotarget 2016;7:25251-63
10. Balaj L, Lessard R, Dai L, Cho YJ, Pomeroy SL, Breakefield XO, *et al.* Tumour microvesicles contain retrotransposon elements and amplified oncogene sequences. Nature communications 2011;2:180
11. Skog J, Wurdinger T, van Rijn S, Meijer DH, Gainche L, Sena-Esteves M, *et al.* Glioblastoma microvesicles transport RNA and proteins that promote tumour growth and provide diagnostic biomarkers. Nat Cell Biol 2008;10:1470-6
12. Peinado H, Lavotshkin S, Lyden D. The secreted factors responsible for pre-metastatic niche formation: old sayings and new thoughts. Seminars in cancer biology 2011;21:139-46
13. Thakur BK, Zhang H, Becker A, Matei I, Huang Y, Costa-Silva B, *et al.* Double-stranded DNA in exosomes: a novel biomarker in cancer detection. Cell research 2014;24:766-9
14. Hoshino A, Costa-Silva B, Shen TL, Rodrigues G, Hashimoto A, Tesic Mark M, *et al.* Tumour exosome integrins determine organotropic metastasis. Nature 2015;527:329-35
15. Syn N, Wang L, Sethi G, Thiery JP, Goh BC. Exosome-Mediated Metastasis: From Epithelial-Mesenchymal Transition to Escape from Immunosurveillance. Trends in pharmacological sciences 2016;37:606-17
16. Rahman MA, Barger JF, Lovat F, Gao M, Otterson GA, Nana-Sinkam P. Lung cancer exosomes as drivers of epithelial mesenchymal transition. Oncotarget 2016;7:54852-66
17. Xiao D, Barry S, Kmetz D, Egger M, Pan J, Rai SN, *et al.* Melanoma cell-derived exosomes promote epithelial-mesenchymal transition in primary melanocytes through paracrine/autocrine signaling in the tumor microenvironment. Cancer letters 2016;376:318-27
18. Costa-Silva B, Aiello NM, Ocean AJ, Singh S, Zhang H, Thakur BK, *et al.* Pancreatic cancer exosomes initiate pre-metastatic niche formation in the liver. Nat Cell Biol 2015;17:816-26
19. Peinado H, Aleckovic M, Lavotshkin S, Matei I, Costa-Silva B, Moreno-Bueno G, *et al.* Melanoma exosomes educate bone marrow progenitor cells toward a pro-metastatic phenotype through MET. Nat Med 2012;18:883-91
20. Zhou W, Fong MY, Min Y, Somlo G, Liu L, Palomares MR, *et al.* Cancer-secreted miR-105 destroys vascular endothelial barriers to promote metastasis. Cancer cell 2014;25:501-15
21. Li SL. [Establishment of a human cancer cell line from adenoid cystic carcinoma of the minor salivary gland]. Zhonghua Kou Qiang Yi Xue Za Zhi 1990;25:29-31, 62
22. Dong L, Wang YX, Li SL, Yu GY, Gan YH, Li D, *et al.* TGF-beta1 promotes migration and invasion of salivary adenoid cystic carcinoma. J Dent Res 2011;90:804-9
23. Marsden CG, Wright MJ, Carrier L, Moroz K, Pochampally R, Rowan BG. "A novel in vivo model for the study of human breast cancer metastasis using primary breast tumor-initiating cells from patient biopsies". BMC cancer 2012;12:10
24. Qu JL, Qu XJ, Qu JL, Qu XJ, Zhao MF, Teng YE, *et al.* The role of cbl family of ubiquitin ligases in gastric cancer exosome-induced apoptosis of Jurkat T cells. Acta Oncol 2009;48:1173-80
25. Lamparski HG, Metha-Damani A, Yao JY, Patel S, Hsu DH, Ruegg C, *et al.* Production and characterization of clinical grade exosomes derived from dendritic cells. J Immunol Methods 2002;270:211-26
26. Grange C, Tapparo M, Collino F, Vitillo L, Damasco C, Deregibus MC, *et al.* Microvesicles released from human renal cancer stem cells stimulate angiogenesis and formation of lung premetastatic niche. Cancer research 2011;71:5346-56
27. Hiratsuka S, Nakamura K, Iwai S, Murakami M, Itoh T, Kijima H, *et al.* MMP9 induction by vascular endothelial growth factor receptor-1 is involved in lung-specific metastasis. Cancer cell 2002;2:289-300
28. Daenen LG, Roodhart JM, van Amersfoort M, Dehnad M, Roessingh W, Ulfman LH, *et al.* Chemotherapy enhances metastasis formation via VEGFR-1-expressing endothelial cells. Cancer research 2011;71:6976-85
29. Kaplan RN, Riba RD, Zacharoulis S, Bramley AH, Vincent L, Costa C, *et al.* VEGFR1-positive haematopoietic bone marrow progenitors initiate the pre-metastatic niche. Nature 2005;438:820-7
30. Li XD, Miao SY, Wang GL, Yang L, Shu YQ, Yin YM. Amphiregulin and epiregulin expression in colorectal carcinoma and the correlation with clinicopathological characteristics. Onkologie 2010;33:353-8
31. Baba I, Shirasawa S, Iwamoto R, Okumura K, Tsunoda T, Nishioka M, *et al.* Involvement of deregulated epiregulin expression in tumorigenesis in vivo through activated Ki-Ras signaling pathway in human colon cancer cells. Cancer research 2000;60:6886-9
32. Kuramochi H, Nakajima G, Kaneko Y, Nakamura A, Inoue Y, Yamamoto M, *et al.* Amphiregulin and Epiregulin mRNA expression in primary colorectal cancer and corresponding liver metastases. BMC cancer 2012;12:88
33. Khambata-Ford S, Garrett CR, Meropol NJ, Basik M, Harbison CT, Wu S, *et al.* Expression of epiregulin and amphiregulin and K-ras mutation status predict disease control in metastatic colorectal cancer patients treated with cetuximab. Journal of clinical oncology : official journal of the American Society of Clinical Oncology 2007;25:3230-7
34. Jing C, Jin YH, You Z, Qiong Q, Jun Z. Prognostic value of amphiregulin and epiregulin mRNA expression in metastatic colorectal cancer patients. Oncotarget 2016;7:55890-9
35. Dong L, Ge XY, Wang YX, Yang LQ, Li SL, Yu GY, *et al.* Transforming growth factor-beta and epithelial-mesenchymal transition are associated with pulmonary metastasis in adenoid cystic carcinoma. Oral Oncol 2013;49:1051-8
36. Jiang Y, Feng X, Zheng L, Li SL, Ge XY, Zhang JG. Thioredoxin 1 mediates TGF-beta-induced epithelial-mesenchymal transition in salivary adenoid cystic carcinoma. Oncotarget 2015;6:25506-19
37. Inaguma S, Kasai K, Ikeda H. GLI1 facilitates the migration and invasion of pancreatic cancer cells through MUC5AC-mediated attenuation of E-cadherin. Oncogene 2011;30:714-23
38. Joost S, Almada LL, Rohnalter V, Holz PS, Vrabel AM, Fernandez-Barrena MG, *et al.* GLI1 inhibition promotes epithelial-to-mesenchymal transition in pancreatic cancer cells. Cancer research 2012;72:88-99
39. Gupta GP, Nguyen DX, Chiang AC, Bos PD, Kim JY, Nadal C, *et al.* Mediators of vascular remodelling co-opted for sequential steps in lung metastasis. Nature 2007;446:765-70
40. Minn AJ, Gupta GP, Siegel PM, Bos PD, Shu W, Giri DD, *et al.* Genes that mediate breast cancer metastasis to lung. Nature 2005;436:518-24
41. Riese DJ, 2nd, Cullum RL. Epiregulin: roles in normal physiology and cancer. Seminars in cell & developmental biology 2014;28:49-56
42. Peinado H, Aleckovic M, Lavotshkin S, Matei I, Costa-Silva B, Moreno-Bueno G, *et al.* Melanoma exosomes educate bone marrow progenitor cells toward a pro-metastatic phenotype through MET. Nature medicine 2012;18:883-91
43. Anklesaria P, Teixido J, Laiho M, Pierce JH, Greenberger JS, Massague J. Cell-cell adhesion mediated by binding of membrane-anchored transforming growth factor alpha to epidermal growth factor receptors promotes cell proliferation. Proc Natl Acad Sci U S A 1990;87:3289-93
44. Park JE, Tan HS, Datta A, Lai RC, Zhang H, Meng W, *et al.* Hypoxic tumor cell modulates its microenvironment to enhance angiogenic and metastatic potential by secretion of proteins and exosomes. Mol Cell Proteomics 2010;9:1085-99
45. He M, Qin H, Poon TC, Sze SC, Ding X, Co NN, *et al.* Hepatocellular carcinoma-derived exosomes promote motility of immortalized hepatocyte through transfer of oncogenic proteins and RNAs. Carcinogenesis 2015;36:1008-18

46. Higginbotham JN, Demory Beckler M, Gephart JD, Franklin JL, Bogatcheva G, Kremers GJ, *et al*. Amphiregulin exosomes increase cancer cell invasion. Current biology : CB 2011;21:779-86